On-chip intermediate potential measurements for the control of electromigration in multi-channel networks in case of time-dependent potential changes

Daniel Sydes[a], Pablo A. Kler[a,b], Peter Zipfl[c], Daniel Lutz[d], Hans Bouwes[e], Carolin Huhn[a]

[a]Institute for Physical and Theoretical Chemistry, Faculty of Science, Eberhard Karls University Tübingen, Germany, [b]Centro de Investigación de Métodos Computacionales (CONICET-UNL), Santa Fe, Argentina, [c]Optoelectronics and Laser Technology Department, University of Applied Sciences Aalen, Aalen, Germany, [d]CalvaSens GmbH, Aalen, Germany and [e]iX-factory GmbH, Dortmund, Germany

Abstract

One of the greatest challenges in multi-channel networks for electromigrative separation techniques is the control of the leakage of sample constituents and band broadening at the channel intersections in microfluidic devices or capillary-chip interfaces, which can be achieved using fixed bias or pullback potentials. These may be implemented as the first separation dimension in a 2D setup, where the electric potential at the interface to the second dimension changes with time. Thus, a dynamic control via on-line potential measurement in combination with a feedback system is needed to control electromigration into the side channels. We here present for the first time a prototype for in-channel potential measurements using a low working current in combination with a Si_3N_4 passivated Ti/Pt electrode at the intersection of the channels in a microfluidic interface. Exemplarily we chose capillary electrophoresis and isotachophoresis as model applications with constant vs. dynamic potential. Parallel on-chip intersection potential measurements were successfully conducted without disturbing capillary zone electrophoretic and isotachophoretic analysis regarding separation and peak performance of amino acids chosen as model analytes. This was possible due to a Si_3N_4 passivation layer, but also due to an ad-hoc developed high impedance instrumentation, resulting in a very low measuring electric current. Simulations of the detected isotachophoretic cross-section potential allowed a deeper understanding of the potential development during the separation.

Keywords

Glass microfluidic interface, capacitively coupled contactless conductivity detection, capillary electrophoresis, isotachophoresis, dynamic electric potential control

1. Introduction

The control of the electric potential at intersections of microfluidic channel networks can enable the feedback control and regulation of electromigration, electroosmosis and thus also separations, mixing processes or the precise split of electroosmotically induced bulk flow. In this manuscript we show the development and application of a prototype for on-chip electric potential measurement. Exemplarily we discuss the possibility to control sample transfer in multidimensional electrophoretic separation techniques in the capillary format that enable analyte pre-concentration, matrix removal and the enhancement of separation peak capacity in case of orthogonal separation mechanisms [1-3]. The coupling of different separations can be accomplished with valves, custom-made interfaces [4,5], microfluidic chips [6-11], as well as capillary-chip hybrid systems and may also include the hyphenation to mass spectrometry (MS) [12-15]. In case of valve-free couplings the greatest challenge is the efficient transfer of sample constituents between channels by using electric fields (electrophoresis and electroosmosis). The fluid velocity field behavior in the region of microchannel intersections has been extensively studied regarding injection strategies and applications for chip platforms [10,16-22]. The most frequent channel intersections used are T- [18], cross- [17,20] or double T-shaped [16] designs. The transfer control is straight-forward if a potential difference is applied only at one channel or capillary, leaving other channels at floating electric potential [23,6]. However, some sample leakage in the order of about 1-3 vol% [18] will occur at the intersection due to hydrodynamic and diffusion effects leading to band broadening and increased detector backgrounds [16]. This leakage can be circumvented using bias or pullback voltages to ensure zero potential difference in the side channels and can easily be achieved by calculating the intersection potential V_i using Ohm's and Kirchhoff's laws in case of buffers of uniform electrical conductivity (such as in CE) [18,24-26].

Further parameters have been shown to account for possible sample leakage: intersection geometry and induced counter pressures [16], length of each connected microchannel, induced junction potentials and field fringing effects at sample buffer interfaces due to

concentration gradients, dispersion effects resulting from differences in the ionic strengths of the solutions used, as well as pressure differences due to zeta potential variations and differing EOF velocities which can lead to pressure-induced volume flows [16,26,27]. Numerical modeling was performed to study the effects responsible for the leakage in detail and therefore develop preventive strategies [28-30]. Data from experimental as well as simulation results show that counter, bias or pullback voltages in combination with a double T or double L geometry of the cross-section are most suitable to minimize leakage effects [22,25,28-32].

These solutions will fail if separation modes like isotachophoresis (ITP) or isoelectric focusing (IEF) using buffer systems with a dynamic variation of the conductivity during the separation process are applied [3,12,33]. The same holds true if a) electrophoresis and electroosmosis are used for mixing or the split of volume flows or when chemical reactions are present and b) if one end of the channel network is at a fixed potential as is the case e.g. when coupled to mass spectrometric detection. In both cases, a control of electromigration and electroosmosis is only achieved if the intersection potential V_i is known and used to continuously adjust the bias potentials at all other channel ends [14].

In this study we introduce - to our knowledge for the first time - a low current in-channel potential measurement, which is applied for ITP and CE applications as well-characterized model applications: A passivated electrode embedded in a microfluidic glass chip [12,13] for interfacing capillary-based multi-dimensional electrophoretic separations was used and applied for on-chip potential measurements for CE and ITP separations of amino acids as model analytes. Numerical simulations are performed for a deeper understanding of the resulting ITP intersection potential measurements.

2. Experimental section

2.1 Materials and methods

Acetic acid (glacial, 100 %), ammonium acetate (≥ 98%), L-arginine monohydrochloride (Arg, for biochemistry) and L-glycine (Gly, ≥ 99.7) were purchased from Merck (Darmstadt, Germany). L-histidine (His, USP grade) was bought from AMRESCO (Solon, Ohio USA). L-

lysine (Lys, ≥ 98%) and isopropanol (LC-MS grade) were from Sigma Aldrich (Steinheim, Germany). All solutions were prepared with doubly-deionized water (Milli-Q purification system from Millipore, Bedford, MA). As leading and terminating electrolyte for ITP experiments, 10 mM ammonium acetate, pH 4.5 (acetic acid) and 28 mM acetic acid, pH 3.2 were used, respectively. This choice for the electrolyte system was made in order to have a fast leading ion (ammonium, absolute electrophoretic mobility=76.2 10^{-9} m^2 V s^{-1}) and the slowest possible terminating ion, which is H^+ for an aqueous electrolyte system. This system gives rise to a wide mobility window including all analytes of interest and showing a large difference in the conductivity, to better study the dynamics of the potential measurements. The background electrolyte (BGE) for CE was 2.3 M acetic acid, pH 2.2 (with the high concentration of the weak acid ensuring buffer capacity). L-histidine and L-arginine 1 mM and L-glycine and L-lysine 0.1 mM solutions were prepared in water as injection solutions for ITP and CE experiments. The high-impedance voltage sensor was connected to the chip electrode by a wire with the conductive carbon glue WireGlue (Anders Products, Melrose, USA).

2.2 Instrumentation

A custom-made multiport HV source (CalvaSens GmbH, Aalen, Germany) enabled the independent operation of 12 high voltage channels, 6 positive (from 0 to 15 kV) and 6 negative (from -15 to 0 kV) [13]. Together with a home-made multi-vial unit this enabled the simultaneous and independent control of pressure and high voltage regimes for up to four vials. Pressure application in the range of 30 mbar to 2 bar for injection and flushing was achieved via the pneumatic unit of an Agilent 7100 CE system (Agilent Technologies, Waldbronn, Germany) by-passing the pneumatic connection of the inlet port via pneumatic valves Festo MFH-3-M5 (FESTO AG, Neuss, Germany) [13] controlled manually with an ad-hoc switch module. Following a previous study [34] the microfluidic borofloat glass chip interface (iX-factory GmbH, Dortmund, Germany) had a cross-channel design with etched channels of 60 µm in width and 25 µm in depth (Figure 1). The thickness of bottom and lid plate were 700 µm and 200 µm. The chip contained an integrated channel electrode made of Ti/Pt for electrically contacting the intersection of the chip channels. The electrode thickness was 15 nm for the titanium and 235 nm for the platinum layer with an additional 500 nm passivation layer of silicon nitride (Si_3N_4).

Silicon nitride deposition was performed with an Oxford PECVD at 300 °C with a RF and LF plasma with an optimized process from the manufacturer in order to avoid pinholes and enhance bonding process quality. PECVD was chosen do to the pre-deposited Ti/Pt electrodes but mostly due to the BF33 glass which has a glass transition temperature of 560°C.

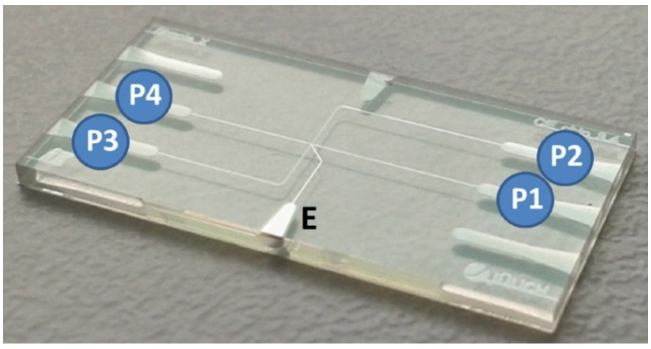

Figure 1: Customized 4 port microfluidic glass chip with a cross-arrangement of the channel network and an integrated Ti/Pt intra-channel electrode (E) for electrically contacting the intersection of the chip channels (iX-factory GmbH, Dortmund, Germany). A 500 nm passivation layer of Si_3N_4 was deposited to electrically passivate the electrode. Chip dimensions were 20 × 10 mm^2. P1-P4 = capillary ports of the chip interface.

Capacitively coupled contactless conductivity detection (C^4D) was performed using an eDAQ ER125 with PowerChrome software Version 2.7.6 (eDAQ Pty Ltd, Denistone East, Australia) using the following parameters: 100 Hz sampling rate, 1200 kHz excitation frequency, 50% amplitude. The electric potential was measured using a home-made high-impedance voltage sensor connected to the chip electrode.

2.3 Numerical simulations

Numerical simulations were performed using a finite element method code using the program PETSc-FEM as platform through a Python interface [35,36]. The simulations were performed on a beowulf cluster at CIMEC using five compute nodes with two quad-core Intel Xeon E5420 2.5 GHz processors, 8 GB DDR3–1333 MHz memory, interconnected via a switched Gigabit Ethernet network [37]. Data postprocessing was performed with Paraview [38], NumPy, SciPy and Matplotlib [39].

2.4 Preparation of the hybrid capillary-chip setup

The fused silica capillaries (50 µm i.d., length 40 cm) were purchased from Polymicro Technologies (Phoenix, AZ), cut to the desired length using a capillary cutter (SHORTIX - Capillary Column Cutter, SGT, The Netherlands and Singapore) and cleaned with isopropanol. The glass chip was cleaned in isopropanol upon ultrasonication for 10 min. Afterwards, the capillaries were glued into the chip capillary ports of the glass chip with epoxy glue. For conditioning the setup was flushed with water and leading electrolyte (for ITP) or background electrolyte (for CE) by pressure application at 2 bar for 10 min. The system was left in doubly-deionized water when not in use. All solutions were introduced via port P1 (see Figure 2).

2.5 ITP and CE conditions

The ITP and CE experiments were conducted in the 1D working mode using two active capillaries with the chip interface in the middle to follow the instantaneous electrical potential during the separation (Figure 2). Port P1 was used for injection and Ports P1 and P4 for the voltage application, while Ports P2 and P3 were blocked with silicone stoppers and left floating during sample injection and separations (see Figure 2A). Model analytes were injected into capillaries filled with BGE (CE) or leading electrolyte (ITP): at a concentration of lysine and glycine of 0.1 mM (CE) or histidine and arginine of 1.0 mM (ITP) for 3 s at 2 bar. For the ITP separation the inlet port P1 contained terminating electrolyte. The separations were performed in triplicate at 11 kV (ITP) or 18 kV (CE) applying 10 kV at the inlet and -1 or -8 kV at the P4 outlet. C^4D detection was accomplished 5 cm after the chip interface. For CE measurements Fast Fourier Transformation smoothing with 25 points was applied (Origin Lab software, Version 9.1) to increase the signal to noise ratio.

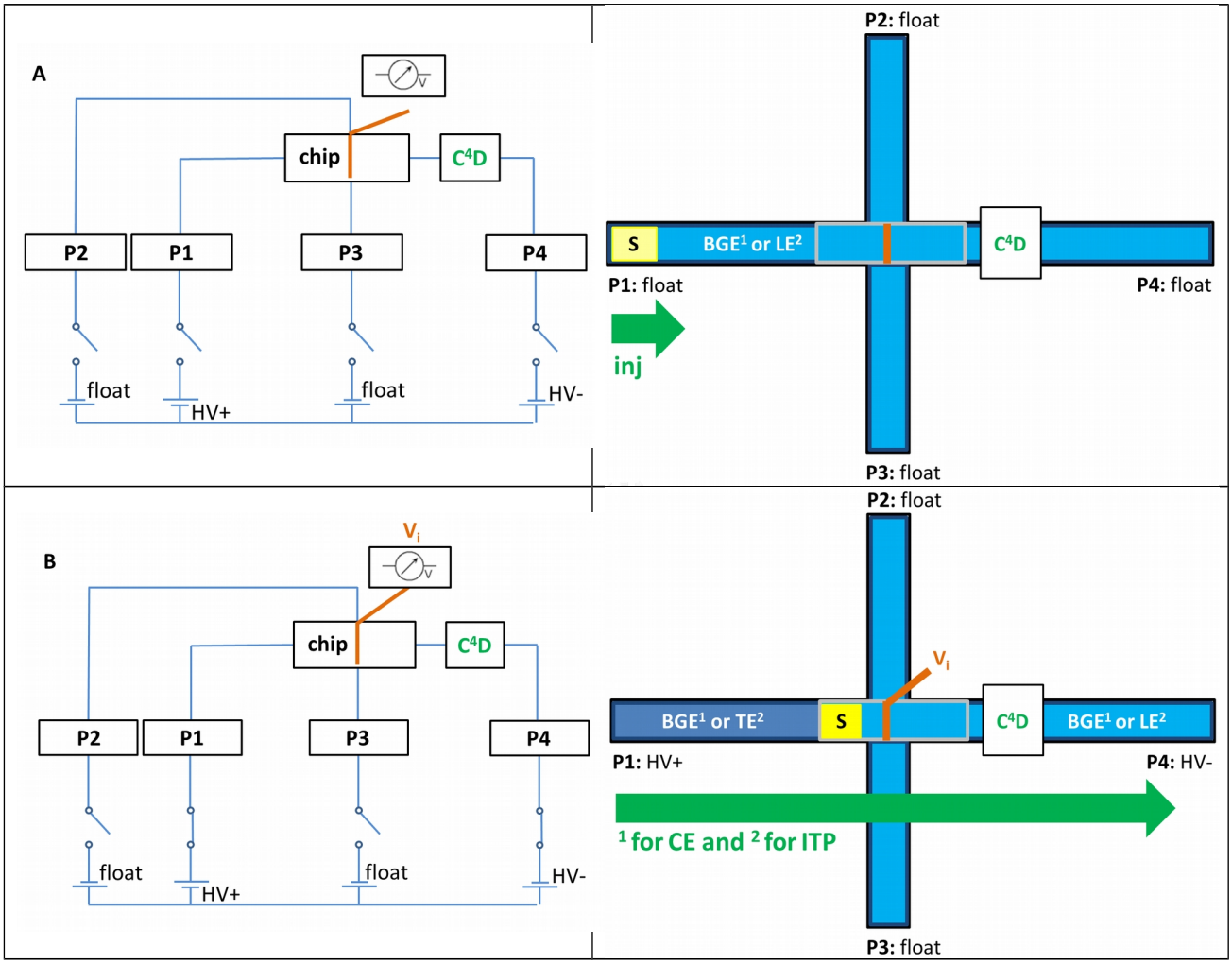

Figure 2: Electrical circuit and operational scheme for the three steps involved in the on-chip potential (V_i) measurements for ITP and CE experiments: P1-4 = ports of the chip interface, S = Sample, inj = Sample injection. **A)** Prior to the sample injection the 2D setup was flushed with BGE or LE, respectively. **B)** After the sample injection step ITP and CE separations were conducted loading the TE or the BGE vial to P1 followed by voltage application to P1 and P4 as well as the on-chip potential measurement.

3. Results and discussion

3.1 General concept of intermediate on-chip cross-section potential measurements

Although several HV sources for multidimensional CE and microchip CE applications were reported [40-42], the problem of monitoring V_i and its implementation has hardly been discussed [41]. In principle, the following basic aspects have to be taken into consideration:

1) Polarizable or conductive materials inside the electric field distort the field lines, which should ideally be parallel to the surface. Charged molecules accumulate on the surface of such materials, and consequently produce a heterogeneous double layer [43]. Thus, a dielectric cover has to shield the intra-channel electrodes to avoid electrical disturbances [44], which we achieve here using a silicon nitride (Si_3N_4) passivation layer over

the electrode made of Ti/Pt, where the Ti layer accounts for enhancing adhesion to the glass and the Pt layer for enhancing electrochemical stability of the contact surface [45]. The choice for Si_3N_4, resulted from a compromise of surface similarity to fused silica as well as enhancement of the chip bonding efficiency [44].

2) In order to avoid electrolysis at the point of potential determination, the electric current intensity circulating through the electrode into the electrolyte should be as low as possible [46]. We here defined a working current of 1-10 nA [47] which results in a low reaction rate (a few femtomoles per second), and a negligible total mass conversion over the whole experiment [48]. In this work, the intersection potential V_i was determined via a high-impedance voltage measurement in the form of a differential measurement of the potential at the intersection vs. a reference potential, determining the final voltage. With the current at the measuring input not exceeding 10 nA and a potential difference on a high common mode voltage range, a very high common mode input impedance is reached. An electronic circuit with explanations is given in the supporting information. The prototype for the potential measurements was optimized to allow measuring with a maximum working current of 10 nA. The technical implementation includes a high-impedance sensor input with a low input capacitance, for the front end of the voltage sensor and a high-voltage field-effect transistor (FET) with a low input capacitance was utilized. A setup in a basic source follower mode provides a common voltage range of approximately ±400 V. This range is clearly not sufficient for the intended operation, therefore, an additional controllable high-voltage supply was utilized in order to track the reference potential of the voltage sensor close to the potential of the passivated sensor electrode. The potential difference of the electrode and the reference should never exceed the common voltage range of the FET front end (i.e. ±400 V) in order to avoid excessive currents flowing through the sensor electrode.

3.2 CE separation of amino acids with parallel on-chip intersection potential measurement

In order to show that the on-chip potential measurements are neither influencing the separation performance nor the analyte peak shapes, amino acid model samples were analyzed with adapted CE [49] and ITP [50] methods, thus comparing separation modes of continuous vs. discontinuous buffer systems. Figure 3 shows the C^4D trace of the electropherograms for the CE separations with and without on-line potential measurements.

Both electropherograms show very good agreement regarding detection time, peak area and peak shape of the two analyzed amino acids.

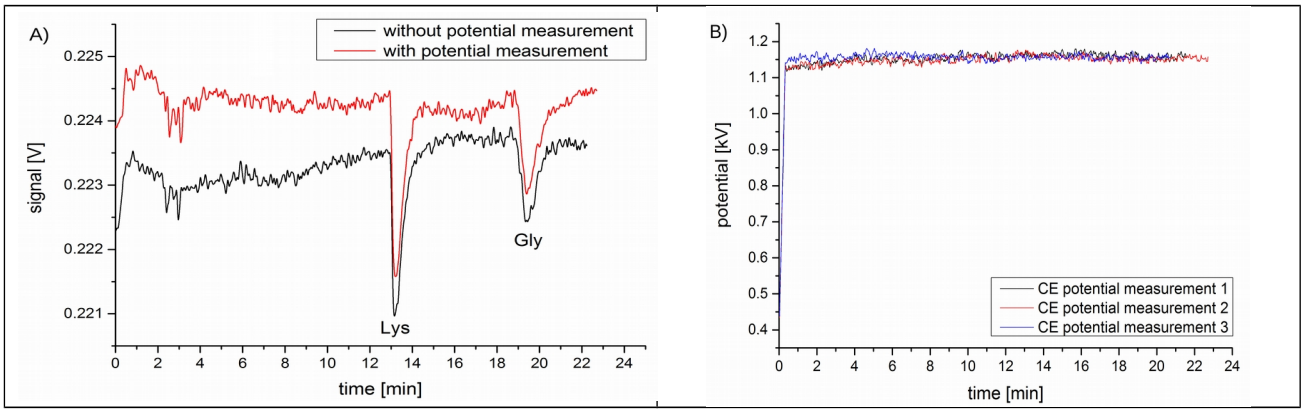

Figure 3: CE separation of Lys and Gly in 2.3 M acetic acid as BGE in the modular hybrid 2D capillary-chip setup at 18 kV. Sample injection at 2 bar for 3 sec from Port 1 (Figure 2). **A)** Electropherograms recorded via a C^4D detector with and without on-chip potential measurement. **B)** On-chip electric potential detection traces.

After the potential increase from voltage ramping during the first 30 sec the measured potential remained stable throughout the whole separation process at 1.18 kV (Figure 2B). The RSD value (n = 3) for the migration time was below 1.5 % and for the peak areas at 11 % and 8 % (Lys and Gly), showing an acceptable precision for the analyte concentrations close to the detection limit. Figure 3B shows on-chip potential measurements with good repeatability of the potential patterns recorded during the 3 CE runs with an RSD value of 1.7 % (averaged potential values over the whole separation time, except the first 30 sec). The RSD values for the noise of the potential signal determined via averaging the values at 10.0 – 10.2 min and 16.6 – 16.8 min with a measuring rate of 1 Hz did not exceed 0.4 %, underlining the stability of the prototype.

3.3 ITP separation of amino acids with on-chip intersection potential measurement

Isotachophoresis is an electromigrative separation techniques which uses a buffer system composed of leading and terminating electrolyte. The sample is injected between these two electrolytes. With the leading electrolyte having a coion to the analyte of highest effective electrophoretic mobility and the terminating electrolyte having a coion of lowest effective electrophoretic mobility, a train-like steady state evolves with a stack of LE-analyte-TE. All

analyte ions sort in the order of decreasing mobility. If a constant current is applied and no electroosmotic flow is present, this stack moves with a constant velocity (at constant voltage, the velocity changes with time). Due to the Kohlrausch regulating function [51], there is a concentration adaptation to the concentration of the leading electrolyte upon passing the original stationary boundary between the samples and the leading electrolyte. A step-shaped isotachopherogram results with the steps idealy composed of a single analyte and the counterion only (plus H^+ or OH^-). During the analysis the leading electrolyte having a high conductivity leaves the separation path while terminating electrolyte enters the capillary so that the overall conductivity over the separation path changes with time.

A very good agreement regarding detection time, ITP step length of the analytes as well as the common step for sodium ions (being an impurity in both sample and terminating electrolyte and being effectively concentrated by ITP), the two analyzed amino acids, as well as the leading and terminating electrolyte zones can be deduced from Figure 4A comparing the isotachopherograms with and without on-line potential measurements. After 30 sec of voltage ramping the potential measured at the intersection reached its highest value of 3.5 kV at the start of the ITP separation (Figure 4B). It then decreased to a minimum of 0.7 kV between 10.0 and 12.5 min but then increased almost linearly from 0.7 kV at 12.5 min to 3.8 kV at 30 min. Further potential application shows asymptotic convergence to a value of ca. 4.2 kV.

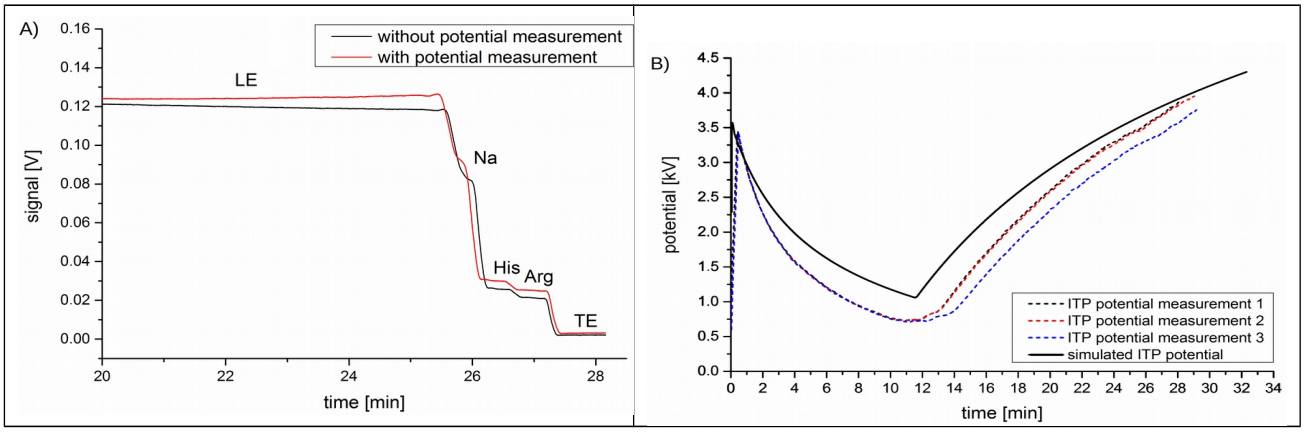

Figure 4: Isotachophoresis of His and Arg in the 1D working mode of the modular 2D capillary-chip setup. LE: 10 mM ammonium acetate, TE: 28 mM acetic acid. Sample injection at 2 bar for 3 sec from Port 1. Separation voltage 18 kV. **A)** C^4D traces of isotachopherograms with and without on-chip potential measurement. **B)** Experimental on-chip potential measurements for ITP-C^4D (n = 3) (dotted

lines) and simulated ITP potential (without electroosmotic effects) under experimental separation conditions (solid line).

Repeatabilities (n = 3) were below 1.4 % for the detection time, and 4 % and 8 % for ITP step lengths of His and Arg. Figure 4B displays three on-chip potential measurements with excellent repeatability of the potential patterns of the first two out of three measurements. The experimental potential patterns showed a good correlation to simulations regarding the time course of the potential (see Figure 4B). The sharp simulation minimum was found at 1.2 kV at a time point of 11.5 min well comparable to the experiment (10.0 - 12.5 min) and the same final value of 4.2 kV as in the experiment. The difference in the sharpness of the minimum of the potential values can be ascribed to the electroosmotic flow (EOF) present in the experiment leading to a bulk flow but not taken into account for the simulation. An additional moving boundary is visible (Figure 5A), which is formed due to the isotachophoretic concentration adaptation of TE: we can expect a zone of the terminator ions with a concentration adapted to the leading ion concentration (following the charge conservation laws for ITP). However, due to electroosmotic bulk flow, also the non-adapted terminator (called TE’ here) from the inlet vial with its original and non-adapted concentration is transported through the capillary and can be detected as a step of conductivities in the boundary TE/TE’ (Figure 5A). A potential value of 4.77 kV is reached when the whole capillary filled with TE’ by applying pressure (2 bar) at the end of the ITP run (Figure 5B), which is well correlated to the change in local conductivity visible in the C^4D trace.

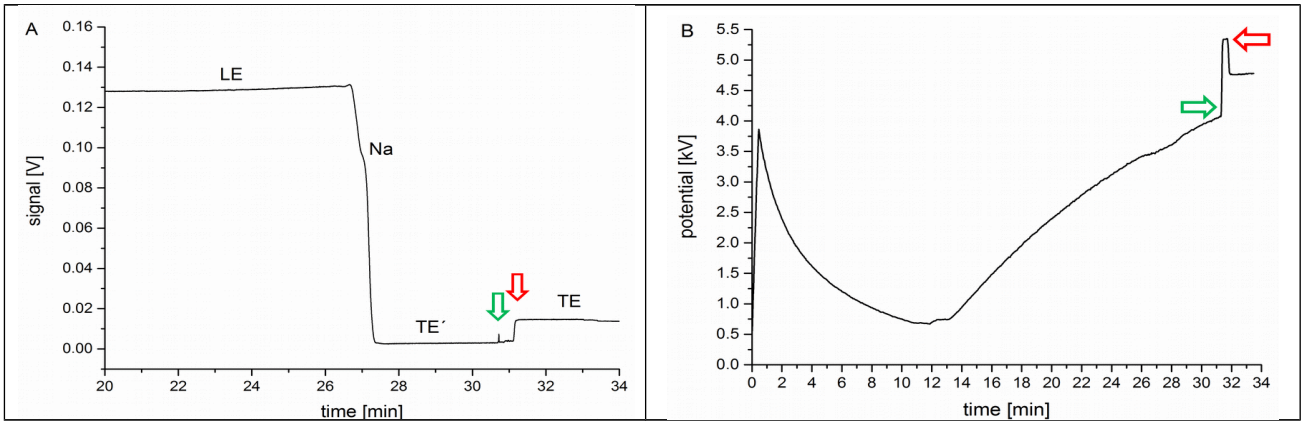

Figure 5: A) C^4D detector signal for on-chip potential measurements for ITP-C^4D (blank run; parameters for the separation were the same as in Figure 4.) **B)** on-chip potential trace; green/red arrow indicate start/stop of pressure application (2 bar).

4. Discussion

The results show that the on-line potential measurements do not disturb CE and ITP separations. No signs of migration time or separation efficiency changes or run failures due to gas bubble formation from electrolysis were visible. After full application of the separation voltage, the measured potential for CE runs stabilized at about +1.18 kV (1.7 % RSD, n = 3) for the whole separation time with very low noise levels. From the difference of the applied separation voltages, +10 kV and -8 kV, a value of +1 kV is expected with the potential measurement electrode placed in the middle of the separation path. The slight offset of +0.18 kV was due to a native component offset of the custom-made multiport HV source. The potential measurement conducted during the separations clearly showed that for uniform buffer systems such as in CE separations (see Figure 3B) the intersection potential is stable throughout the whole separation process as expected, thus demonstrating the feasibility of the presented on-chip potential measurements. The prototype can thus be used for the control of the potential difference in side channel or even pinched injection modes [17].

The system also proved to be able to determine the dynamic potential changes due to conductivity changes in ITP. The high correlation of the repetitive measurements also during the first 30 sec of increasing potential during voltage ramping is worth to be noticed pointing to a highly dynamic reaction towards potential changes. Furthermore, the prototype will also be applicable when fixed potential e.g. ground potential in the hyphenation to MS is used. It is then possible to continuously adapt the bias voltages to electrokinetically close

separation channels and thus reduce sample leakage at channel interfaces or controlling mixing and reaction processes as well as splitting of volume flow in electric fields.

From the simulation results given in Figure 4B in comparison to the experimental results it is clear that the prototype adequately follows the dynamic potential changes in the system. The potential decline after application of full separation voltage for the ITP experiments is exponential due to the very fast migration of the leading electrolyte front within the capillary and is slowed down progressively with separation time because of the entrance of the adapted and non-adapted terminating electrolyte front into the separation channel. The minimum electric potential is reached when the capillary portion between P1 and the electrode is filled with TE (half of the capillary for a symmetric setup, as in our case), thus, when the sample zone is present in the interface. The broadness of the minimum correlates with the detected ITP sample stack and therefore depends on its length. The ITP sample plug length detected via the conductivity detector is 2 min (25.5 to 27.5 min, see Figure 4A) and the width of the potential minimum ca. 2.5 min (see Figure 4B). Therefore, in this example the on-chip potential measurements can complement on-chip [13] or intermediate [9,12] C^4D measurements for sample transfer in 2D setups [1,12,13]. The further potential changes after 13.3 min are related to filling the second capillary with TE.

This filling takes longer than at the beginning of the separation as evident from the shown potential increase, due to the lower mobility of the terminating electrolyte (ITP separations were conducted at constant separation voltage, were velocity changes occur upon the progress of the separation). A final potential of 4.5 kV is expected for a separation path homogeneously filled with concentration-adapted TE´ with separation voltages of +10 kV and -1 kV at Ports 1 and 4. For the simulations as well as for the experimental data a final potential of approximately 4 kV was obtained. The difference of 0.5 kV at the minimum is due to the non-adapted TE zone entering the capillary due to EOF (not considered in the numerical simulations), resulting in a slightly non-uniform TE/TE´ zone [52]. As for the CE experiments, the offset of +0.27 kV is due to the component uncertainty of the custom-made multiport HV source.

5. Conclusion and outlook

We here present a device for intersection potential measurements targeted to control electromigration and electroosmosis in multichannel networks, exemplarily shown for capillary electrophoresis and isotachophoresis with the aim to control sample transfer in multi-dimensional electrophoretic separations using a low current measuring prototype in combination with a Si_3N_4 passivated Ti/Pt electrode inside a glass microfluidic interface. On-chip intersection potential measurements were successfully conducted without disturbing electrolyte conditions and thus CE and ITP analysis regarding separation and peak shape efficiency. The results obtained underline the excellent stability of the potential measurement and the suitability of the passivation of the electrode clearly avoiding disturbances of the electric field lines as well as electrolysis during potential measurements e.g. conducted during electrophoretic separations. Successful simulation of the detected ITP intersection potential allowed a deeper understanding of the potential development during the separation and corroborated the experimental findings. The gradual exit of the leading electrolyte and the entrance of the adapted terminating electrolyte were monitored by potential changes.

In order to accomplish a feedback system of potential adjustment by using bias voltages, a future development will be a software-controlled electrical feedback regulation of the applied potential via different HV power supplies to be implemented in the presented setup. With this combination it will be possible to electrokinetically close side channels and enable the hyphenation to systems at fixed potentials, e.g. mass spectrometry. Finally, It is worth to mention that the presented system is able to measure intermediate electric potential for any other microfluidic application that involves the external application of an electric field, i.e. dielectrophorectic processes, electrochemical reactions, electrowetting, among others.

Acknowledgements

We thank the German Excellence Initiative commissioned by the German Research Foundation (DFG) for financial support. The ITP simulations were partly conducted during a study stay of Daniel Sydes at CIMEC in the working group of Pablo A. Kler in Argentina financed by a doctoral scholarship from the German Academic Exchange Service (DAAD)

from the 14th of April till 30th of June 2015. Daniel Sydes wants to thank the DAAD for funding.

References

[1] P.A. Kler, D. Sydes, C. Huhn, Column–coupling strategies for multidimensional electrophoretic separation techniques, Anal. Bioanal. Chem. 407 (2015) 119–138.

[2] F.J. Kohl, L. Sánchez-Hernández, C. Neusüß, Capillary electrophoresis in two-dimensional separation systems: Techniques and applications., Electrophoresis, 36 (2015) 144–158.

[3] P. Mikuš, K. Marákova, Column coupling electrophoresis in biomedical analysis, biomedical engineering - from theory to applications, Fazel R. (Eds.), InTech: Rijeka, 2011, 81–130.

[4] D. Mohan, L. Pasă-Tolić, C.D. Masselon, N. Tolić, B. Bogdanov, K.K. Hixson, R.D. Smith, C.S. Lee, Integration of electrokinetic-based multidimensional separation/concentration platform with electrospray ionization-fourier transform ion cyclotron resonance-mass spectrometry for proteome analysis of *Shewanella oneidensis*, Anal. Chem. 75 (2003) 4432–4440.

[5] J.A. Dickerson, L.M. Ramsay, O.O. Dada, N. Cermak, N.J. Dovichi, Two-dimensional capillary electrophoresis: capillary isoelectric focusing and capillary zone electrophoresis with laser-induced fluorescence detection, Electrophoresis 31 (2010) 2650–2654.

[6] Y. Cong, L. Zhang, D. Tao, Y. Liang, W. Zhang, Y. Zhang, Miniaturized two-dimensional capillary electrophoresis on a microchip for analysis of the tryptic digest of proteins, J. Sep. Sci. 31 (2008) 588–594.

[7] H. Shadpour, S.A. Soper, Two-dimensional electrophoretic separation of proteins using poly(methyl methacrylate) microchips, Anal. Chem. 78 (2006) 3519–3527.

[8] A.E. Herr, J.I. Molho, K.A. Drouvalakis, J.C. Mikkelsen, P.J. Utz, J.G. Santiago, T.W. Kenny, On-chip coupling of isoelectric focusing and free solution electrophoresis for multidimensional separations, Anal. Chem. 75 (2003) 1180–1187.

[9] Y.C. Wang, M.H. Choi, J. Han, Two-dimensional protein separation with advanced sample and buffer isolation using microfluidic valves, Anal. Chem. 76 (2004) 4426–2231.

[10] G.J.M. Bruin, Recent developments in electrokinetically driven analysis on microfabricated devices, Electrophoresis 21 (2000) 3931–3951.

[11] R. Bodor, D. Kaniansky, M. Masár, K. Silleová, B. Stanislawski, Determination of bromate in drinking water by zone electrophoresis-isotachophoresis on a column-coupling chip with conductivity detection, Electrophoresis 23 (2002) 3630–3637.

[12] P.A. Kler, T.N. Posch, M. Pattky, R.M. Tiggelaar, C. Huhn, Column coupling isotachophoresis-capillary electrophoresis with mass spectrometric detection: Characterization and optimization of microfluidic interfaces, J. Chromatogr. A 1297 (2013) 204–212.

[13] P.A. Kler, C. Huhn, Non-aqueous electrolytes for isotachophoresis of weak bases and its application to the comprehensive preconcentration of the 20 proteinogenic amino acids in column-coupling ITP/CE–MS, Anal. Bioanal. Chem. 406 (2014) 7163–7174.

[14] R. Tomáš, K. Klepárník, F. Foret, Multidimensional liquid phase separations for mass spectrometry, J. Sep. Sci. 31 (2008) 1964–1979.

[15] J.J. Lu, S. Wang, G. Li, W. Wang, Q. Pu, S. Liu, Chip-capillary hybrid device for automated transfer of sample preseparated by capillary isoelectric focusing to parallel capillary gel electrophoresis for two-dimensional protein separation, Anal. Chem. 84 (2012) 7001–7007.

[16] L.L. Shultz-Lockyear, L. Christa, C.L. Colyer, Z.H. Fan, K.I. Roy, D.J. Harrison, Effects of injector geometry and sample matrix on injection and sample loading in integrated capillary electrophoresis devices, Electrophoresis 20 (1999) 529–538.

[17] J.P. Alarie, S.C. Jacobson, C.T. Culbertson, J.M. Ramsey, Effects of the electric field distribution on microchip valving performance, Electrophoresis 21 (2000) 100–106.

[18] K. Seiler, Z.H. Fan, K. Fluri, D.J. Harrison, Electroosmotic pumping and valveless control of fluid flow within a manifold of capillaries on a glass chip, Anal. Chem. 66 (1994) 3485–3491.

[19] D.J. Harrison, K. Fluri, K. Seiler, Z.H. Fan, C.S. Effenhauser, A. Manz, Micromachining a miniaturized capillary electrophoresis-based chemical analysis system on a chip, Science 261 (1993) 895–897.

[20] Z.H. Fan, D.J. Harrison, Micromachining of capillary electrophoresis injectors and separators on glass chips and evaluation of flow at capillary intersections, Anal. Chem. 66 (1994) 177–184.

[21] D. Belder, M. Ludwig, Microchip electrophoresis for chiral separations, Electrophoresis 24 (2003) 2422–2430.

[22] B.W. Wenclawiak, R.J. Püschl, Sample injection for capillary electrophoresis on a micro fabricated device/on chip CE injection, Anal. Lett. 39 (2006) 3–16.

[23] C.L.A. Berli, Equivalent circuit modeling of electrokinetically driven analytical microsystems, Microfluid. Nanofluid. 4 (2008) 391–399.

[24] S.C. Jacobson, S.V. Ermakov, J.M. Ramsey, Minimizing the number of voltage sources and fluid reservoirs for electrokinetic valving in microfluidic devices, Anal. Chem. 71 (1999) 3273–3276.

[25] L.M. Fu, J.C. Leong, C.F. Lin, C.H. Tai, Tsai C.H., High performance microfluidic capillary electrophoresis devices, Biomed. Microdevices 9 (2007) 405–412.

[26] H.J. Crabtree, E.C.S. Cheong, D.A. Tilroe, C.J. Backhouse, Microchip injection and separation anomalies due to pressure effects, Anal. Chem. 73 (2001) 4079–4086.

[27] E.V. Dose, G. Guiochon, Problems of quantitative injection in capillary zone electrophoresis, Anal. Chem. 64 (1992) 123–128.

[28] F. Bianchi, R. Ferrigno, H.H. Girault, Finite element simulation of an electroosmotic-driven flow division at a T-junction of microscale dimensions, Anal. Chem. 72 (2000) 1987–1993.

[29] C.H. Tsai, R.J. Yang, C.H. Tai, L.M. Fu, Numerical simulation of electrokinetic injection techniques in capillary electrophoresis microchips, Electrophoresis 26 (2005) 674–686.

[30] L.M. Fu, C.H. Lin, Numerical Analysis and Experimental Estimation of a Low-Leakage Injection Technique for Capillary Electrophoresis, Anal. Chem. 75 (2003) 5790–5796.

[31] C.H. Lin, R.J. Yang, C.H. Tai, C.Y. Lee, L.M. Fu, Double-L injection technique for high performance capillary electrophoresis detection in microfluidic chips, J. Micromech. Microeng. 14 (2004) 639–646.

[32] C.H. Tsai, Y.N. Wang, C.F. Lin, R.J. Yang, L.M. Fu, Experimental and numerical investigation into leakage effect in injectors of microfluidic devices, Electrophoresis 27 (2006) 4991–4998.

[33] J. Hühner, M. Lämmerhofer, C. Neusüß, Capillary isoelectric focusing-mass spectrometry: Coupling strategies and applications, Electrophoresis 36 (2015) 2670–2686 .

[34] R. Tiggelaar, F. Benito-Lopez, D. Hermes, H. Rathgen, R. Egberink, F. Mugele, D. Reinhoudt, A. van den Berg, W. Verboom, H. Gardeniers, Fabrication, mechanical testing and application of high-pressure glass microreactor chips, Chem. Eng. J. 131 (2007) 163–170.

[35] P.A. Kler, L.D. Dalcin, R.R. Paz, T.E. Tezduyar, SUPG and discontinuity-capturing methods for coupled fluid mechanics and electrochemical transport problems, Comput. Mech. 51 (2013) 171–185.

[36] P.A. Kler, C.L.A. Berli, F.A. Guarnieri, Modeling and high performance simulation of electrophoretic techniques in microfluidic chips, Microfluid. Nanofluid. 10 (2011) 187–198.

[37] L.D. Dalcin, R.R. Paz, P.A. Kler, A. Cosimo, Parallel distributed computing using Python, Adv. Water Resour. 34 (2011) 1124–1139.

[38] U. Ayachit, The ParaView Guide: A parallel visualization application, Kitware Inc., 2015.

[39] S. van der Walt, S.C. Colbert, G. Varoquaux, The NumPy Array: A structure for efficient numerical computation, Comput. Sci. Eng. 13 (2011) 22–30.

[40] J.L. Felhofer, L. Blanes, C.D. Garcia, Recent developments in instrumentation for capillary electrophoresis and microchip-capillary electrophoresis, Electrophoresis 31 (2010) 2469–2486.

[41] L. Jiang, X. Jiang, Y. Lu, Z. Dai, M. Xie, J. Qin, B. Lin, Development of a universal serial bus-powered mini-high-voltage power supply for microchip electrophoresis, Electrophoresis 28 (2007) 1259–1264.

[42] Q. Li, H. Zhang, Y. Wang, B. Tang, X. Liu, X. Gong, Versatile programmable eight-path-electrode power supply for automatic manipulating microfluids of a microfluidic chip, Sens. Actuators, B 136 (2009) 265–274.

[43] F. Zhang, Y. Daghighi, D. Li, Control of flow rate and concentration in microchannel branches by induced-charge electrokinetic flow, J. Colloid Interf. Sci. 364 (2011) 588–593.

[44] S. Shin, B.S. Kim, J. Song, H. Lee, H.H. Cho, A facile route for the fabrication of large-scale gate-all-around nanofluidic field-effect transistors with low leakage current, Lab Chip 12 (2012) 2568–2574.

[45] M.J. Madou, Fundamentals of Microfabrication: The science of miniaturization, 2nd ed., CRC Press LLC: Boca Raton, 2002.

[46] Y.J. Oh, D. Bottenus, C.F. Ivory, S.M. Han, Impact of leakage current and electrolysis on FET flow control and pH changes in nanofluidic channels, Lab Chip 9 (2009) 1609–1617.

[47] R.S. Keynton, T.J. Roussel Jr., M.M. Crain, D.J. Jackson, D.B. Franco, J.F. Naber, K.M. Walsh, R.P. Baldwin, Design and development of microfabricated capillary electrophoresis devices with electrochemical detection, Anal. Chim. Acta 507 (2004) 95–105.

[48] R.S. Martin, Interfacing amperometric detection with microchip capillary electrophoresis, Methods Mol. Biol. 339 (2006) 85–112.

[49] P. Coufal, J. Zuska, T. van de Goor, V. Smith, B. Gaš, Separation of twenty underivatized essential amino acids by capillary zone electrophoresis with contactless conductivity detection, Electrophoresis 24 (2003) 671–677.

[50] P. Kubačák, P. Mikuš, I. Valášková, E. Havránek, Simultaneous determination of essential basic amino acids in pharmaceuticals by capillary isotachophoresis, Arch. Pharm. Chem. Life Sci. 339 (2006) 96–99.

[51] P. Bocek, M. Deml, P. Gebauer, and V. Dolnik, Analytical Isotachophoresis, VCH Publishers, Weinheim, 1988.

[52] J.L. Beckers, F.M. Everaerts, M.T. Ackermans, Isotachophoresis with electroosmotic flow: open *versus* closed systems, J. Chromatogr. 537 (1991) 429–442.